Engineering of Electron-Selective Contact for Perovskite Solar Cells with Efficiency Exceeding 15%

Qin Hu,[†] Jiang Wu,[†] Chang Jiang,[†] Tanghao Liu,[†] Xinglu Que,[†] Rui Zhu,[*,†,‡] and Qihuang Gong[*,†,‡]

[†]State Key Laboratory for Artificial Microstructure and Mesoscopic Physics, School of Physics, Peking University, Beijing 100871, China and [‡]Collaborative Innovation Center of Quantum Matter, Beijing 100871, China

ABSTRACT The past 5 years have witnessed the rise of highly efficient organometal halide perovskite-based solar cells. In conventional perovskite solar cells, compact n-type metal oxide film is always required as a blocking layer on the transparent conducting oxide (TCO) substrate for efficient electron-selective contact. In this work, an interface engineering approach is demonstrated to avoid the deposition of compact n-type metal oxide blocking film. Alkali salt solution was used to modify the TCO surface to achieve the optimized interface energy level alignment, resulting in efficient electron-selective contact. A remarkable power conversion efficiency of 15.1% was achieved under AM 1.5G 100 mW·cm^{-2} irradiation without the use of compact n-type metal oxide blocking layers.

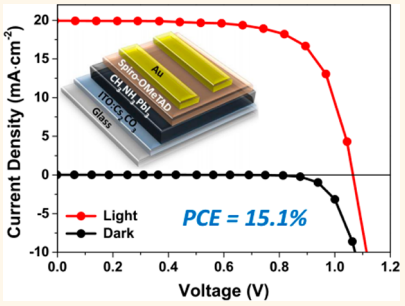

KEYWORDS: electron-selective contact · perovskite solar cells · interface engineering

During the past decades, next-generation photovoltaic (PV) devices have attracted increasing interests around the world. Several promising candidates[1] have been extensively studied with the aim to improve power conversion efficiency (PCE), reduce device cost, and enhance device stability, *etc*. These candidates include organic bulk heterojunction solar cells, quantum dot solar cells, kesterite thin-film solar cells, and dye-sensitized solar cells (DSSCs), *etc*. Considerable progress has been made for these PV technologies, with remarkable device performance achieved.[1]

Since 2009, a novel alternative PV technology, perovskite-based solar cells, has become a rapidly rising star for next-generation PV technologies.[2−8] Evolving from DSSCs, a perovskite solar cell is organic−inorganic hybrid PV technology, which uses organometal halide perovskite compounds as light absorbers. Organometal halide perovskites, for example, $CH_3NH_3PbI_3$, were first used as visible-light sensitizers in liquid-electrolyte-based DSSCs in 2009,[9] with a modest PCE of 3.8%. Significant performance boosts were then achieved by incorporating a perovskite active layer into a solid-state hybrid device architecture.[10,11] The perovskite layer was sandwiched between a compact electron-selective contact and an organic hole-selective contact,[12] resulting in perovskite solar cells with PCEs of ∼10%. Further optimization of device fabrication processes has pushed the PCE up to ∼15%.[13−16] Most recently, a PCE of 17.9% has been reported and certified for perovskite solar cells.[17] Moreover, it was also predicted that the PCE of perovskite solar cells could approach 20% in the next couple of years,[2,3] indicating its great potential for future low-cost PV technology.

As mentioned above, in conventional perovskite solar cells, a compact n-type metal oxide film is always required on the transparent conducting oxide (TCO) substrate as a blocking layer for electron-selective contacts (ESCs). This thin blocking layer could prevent direct contact between the TCO and hole-transporting materials.[18] The most commonly used compact n-type metal oxide is TiO_2, which is deposited through aerosol spray pyrolysis[10,19] or spin-coating methods.[20,21] High-temperature annealing is often required to achieve a relatively compact or dense structure. This is not compatible with a plastic substrate and unfavorable for low-cost fabrication processes.[15] To avoid high-temperature processes for the compact ESCs, several approaches have been demonstrated with considerable device

* Address correspondence to iamzhurui@pku.edu.cn, qhgong@pku.edu.cn.

Received for review June 2, 2014 and accepted September 26, 2014.

Published online September 26, 2014
10.1021/nn5029828

performance. For example, graphene was incorporated with the low-temperature processed TiO_2 nanoparticles,[22] giving a nanocomposite electron collection layer in the perovskite solar cell. The superior charge collection induced by graphene in the nanocomposite could enable the device fabrication processes at temperatures no higher than 150 °C. Remarkable PV performance was achieved with a PCE of up to 15.6%. Crystalline anatase TiO_2 nanoparticles were also demonstrated to achieve compact ESCs through low-temperature processes (<150 °C).[16] A maximum PCE of 15.9% was achieved under standard testing conditions. In addition to TiO_2-based n-type materials, ZnO was recently shown to be a good candidate for ESCs in perovskite solar cells.[15,23] ZnO is known to have superior electron mobility.[24] The solution-processed ZnO nanoparticles were found to form a relatively compact film without sintering steps. Perovskite solar cells utilizing ZnO compact film could reach a PCE close to 16% under standard simulated solar illumination.[15]

In addition to n-type metal oxide materials, efforts were also made to utilize other organic or inorganic materials for electron-selective contact, such as [6,6]-phenyl-C_{61}-butyric acid methyl ($PC_{61}BM$), poly[(9,9-bis(3′-(*N*,*N*-dimethylamino)propyl)-2,7-fluorene)-*alt*-2,7-(9,9-dioctylfluorene)] (PFN),[25] and CdS,[26] *etc*; however, no remarkable device performance was reported based on these ESCs. In this work, a surface modification approach is demonstrated to achieve efficient ESCs in perovskite solar cells. Cesium carbonate solution was used to modify an indium−tin−oxide (ITO) surface, leading to the optimized interface energy level alignment between ITO and perovskite light absorber. Results indicated that cesium salt solution treatment did not form a visible compact cesium salt layer on ITO; however, a remarkable PCE of 15.1% could still be achieved under AM 1.5G 100 $mW \cdot cm^{-2}$ irradiation as the result of interface energy level engineering. This provides an example of efficient perovskite solar cells without the deposition of a compact n-type metal oxide electron-selective layer. Furthermore, the results also reveal that interface engineering strategies could be effectively utilized to realize the efficient perovskite solar cells with the aim of achieving PCE exceeding 20%.[2,3]

RESULTS AND DISCUSSION

Figure 1a shows the device configuration of the perovskite solar cells based on electron-selective contact engineering. The device fabrication was performed on the ITO substrate, which is suitable for low-temperature processes. Cs_2CO_3 solution was used to modify the surface of ITO. This surface treatment was repeated for varied times to ensure the desired surface modification. A perovskite active layer was deposited onto the Cs_2CO_3-modified ITO substrate (referred to as ITO:Cs_2CO_3) through a sequential deposition process. Then, p-type 2,2′,7,7′-tetrakis[*N*,*N*-di(4-methoxyphenyl)-amino]-9,9′-spirobifluorene (Spiro-OMeTAD) was coated onto the perovskite active layer as a hole conductor. The device was finalized by depositing Au as top contact electrode. Figure 1b shows the cross-sectional image of a finished device. From the cross-sectional image, no additional blocking layer is clearly visible between the perovskite layer and the ITO substrate, indicating that the Cs_2CO_3 did not form a visible compact structure.

The Cs_2CO_3-modified ITO surfaces were then investigated by scanning electron microscopy (SEM).

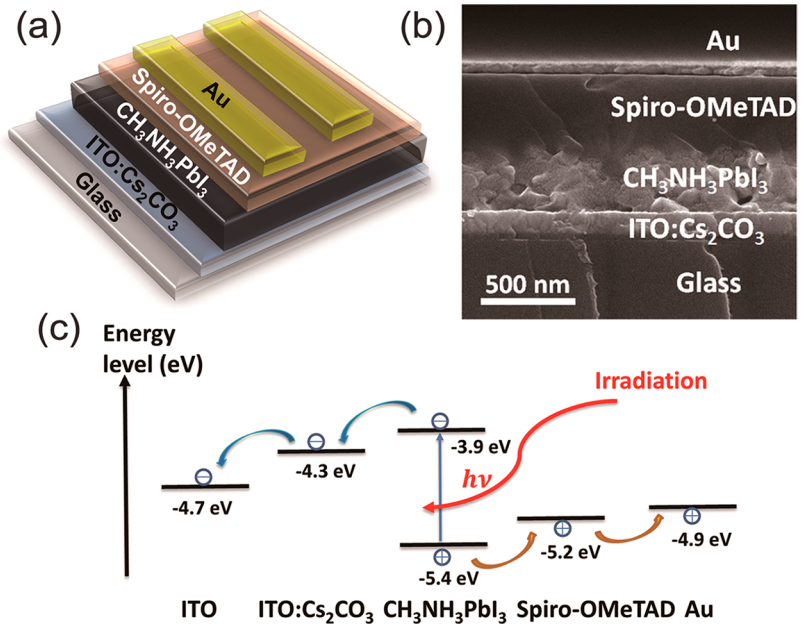

Figure 1. Device architecture. (a) Schematic of the device structure. (b) SEM cross-sectional image of a perovskite solar cell based on Cs_2CO_3-modified ITO substrate. (c) Energy level diagram.

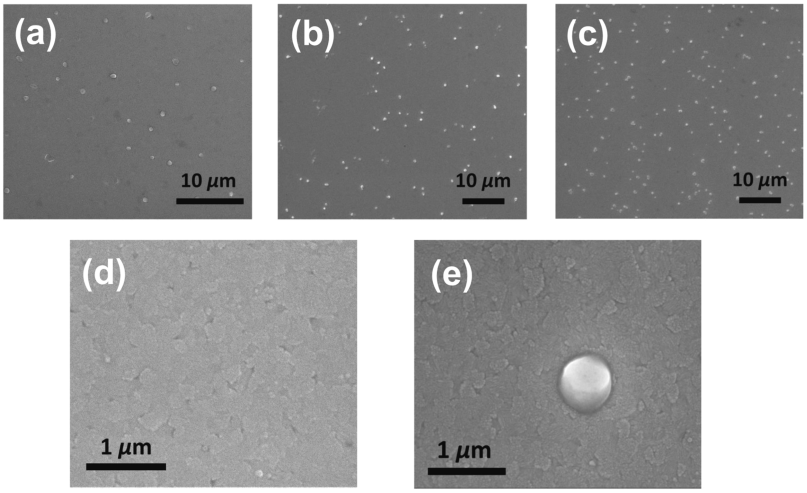

Figure 2. Scanning electron microscopy images for Cs_2CO_3-modified ITO. ITO surfaces were modified by Cs_2CO_3 solution for (a) one, (b) two, and (c) three times. Enlarged SEM images compared the surface morphologies of pristine (d) ITO and (e) Cs_2CO_3-modified ITO (3 times).

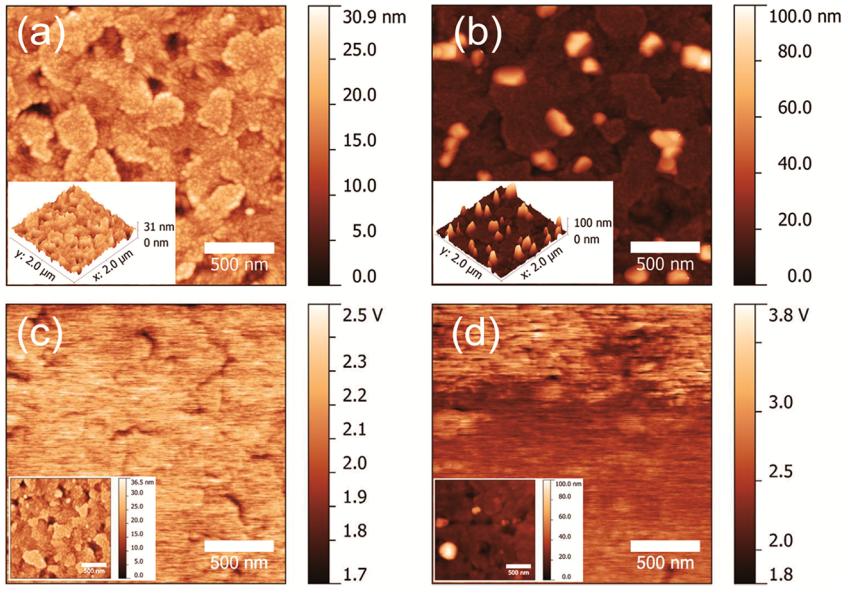

Figure 3. Atomic force microscopy images and Kelvin probe force microscopy images. ITO surface (a) before and (b) after Cs_2CO_3 treatment. Inset: Three-dimensional surface topographical images. Surface potential images of (c) ITO and (d) ITO: Cs_2CO_3. Inset: Topography images.

Figure 2a–c compares the SEM images of ITO surfaces after being treated by Cs_2CO_3 solution one, two, and three times. According to the SEM images, Cs_2CO_3 salt precipitated and aggregated to form sub-microscale spots on the ITO surface after solvent evaporation. The density of Cs_2CO_3 spots increased along with the treatment times, forming discontinuous islands. Figure 2d,e compares the enlarged SEM images for the surfaces of pristine ITO or the ITO after three treatments. From Figure 2e, it can be observed that the surface morphology around a Cs_2CO_3 spot is similar to that of the pristine ITO surface. This confirms that the Cs_2CO_3 did not form a continuous compact film on the ITO surface. The surface morphologies were further investigated by atomic force microscopy (AFM).

Figure 3 shows the surface topographical images comparing the ITO surfaces before and after Cs_2CO_3 treatment. For the pristine ITO surface, the surface roughness values of the arithmetic average (R_a) and the root mean square (R_q) are 2.61 and 3.40 nm for the whole scanned area (Figure 3a). After Cs_2CO_3 treatment, the sub-microscale spots formed with heights ranging from 50 to 100 nm. However, R_a and R_q of the areas excluding Cs_2CO_3 spots were 2.61 and 3.65 nm (Figure 3b), which were similar to those of pristine ITO. These results were consistent with the SEM images in Figure 2.

In order to explore the best Cs_2CO_3 treatment conditions, varied coating times were performed on ITO. Photovoltaic performances of the perovskite solar

TABLE 1. Performance Summary of the Perovskite Solar Cells Based on Different Electron-Selective Contacts[a]

electron-selective contact	V_{oc} (V)	J_{sc} (mA·cm^{-2})	FF	PCE (%)
pristine ITO	0.90	13.3	0.36	4.3
ITO:Cs_2CO_3 (1 time)	0.96	17.8	0.57	9.7
ITO:Cs_2CO_3 (2 times)	1.02	18.7	0.64	12.2
ITO:Cs_2CO_3 (3 times)	1.05	19.1	0.72	14.4
ITO:Cs_2CO_3 (4 times)	1.03	19.0	0.69	13.5
ZnO (sol−gel)	1.01	20.4	0.66	13.6
TiO_2 (spray pyrolysis)	1.07	20.1	0.66	14.2

[a] Device performance was measured under AM 1.5G 100 mW·cm^{-2} illumination.

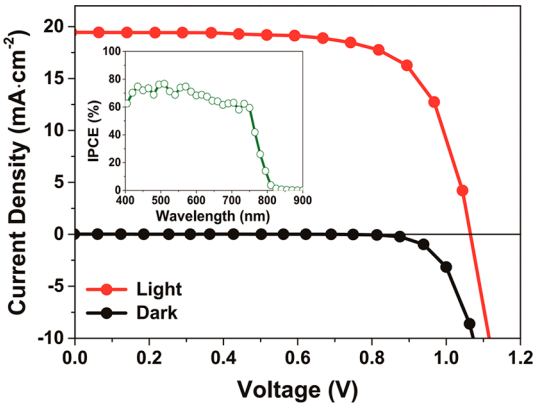

Figure 4. Photovoltaic performance characterization. The best performance achieved for the perovskite solar cells fabricated on the Cs_2CO_3-modified ITO substrates. Inset: IPCE spectrum for the same device.

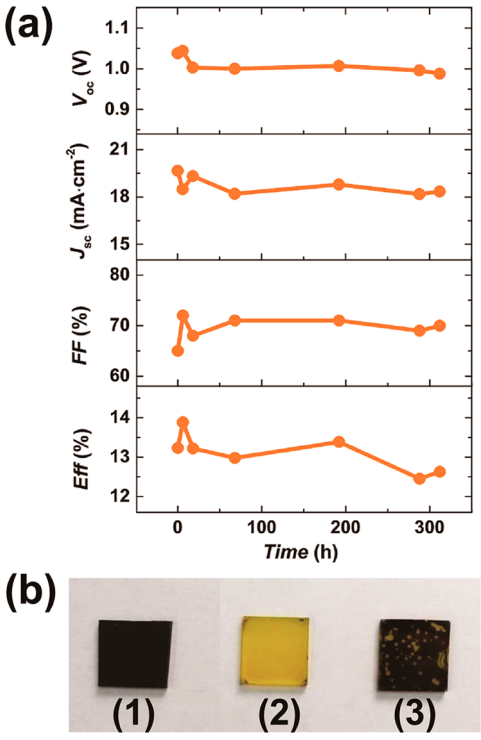

Figure 5. Stability test. (a) Photovoltaic performance stability of the devices using Cs_2CO_3-modified ITO as electron-selective contact. (b) Thermal stability test of the $CH_3NH_3PbI_3$ films deposited on the Cs_2CO_3-modified or ZnO-coated ITO substrates. The annealing conditions are (b1) ITO:Cs_2CO_3/$CH_3NH_3PbI_3$, 130 °C, 30 min; (b2) ITO:ZnO/$CH_3NH_3PbI_3$, 130 °C, 5 min; (b3) ITO:ZnO/$CH_3NH_3PbI_3$, 80 °C, 60 min.

cells based on these electron-selective contacts were investigated. Table 1 summarizes the device performance measured under simulated AM 1.5G 100 mW·cm^{-2} illumination. The device fabrication processes were well-controlled with only variations in ESCs. For the device without Cs_2CO_3 treatment, poor performance was obtained. The device performance became better as long as the Cs_2CO_3 treatment times increased. The best performance could be reached when ITO was treated by Cs_2CO_3 solution for three times. An open-circuit voltage (V_{oc}) of 1.05 V, short-circuit current density (J_{sc}) of 19.1 mA·cm^{-2}, and fill factor (FF) of 0.72 were achieved, resulting in power conversion efficiency of 14.4%. Further increase in treating times did not show improvement in device performance. Based on the Cs_2CO_3-modified ITO substrates (3 times), the champion PCE of 15.1% was achieved, with a V_{oc} of 1.07 V, J_{sc} of 19.9 mA·cm^{-2}, and FF of 0.71, as shown in Figure 4. Incident photon-to-current conversion efficiency (IPCE) spectrum was also obtained (inset of Figure 4). The J_{sc} calculated from the IPCE spectrum is 18.6 mA·cm^{-2}, which agrees with the J_{sc} measured from $J-V$ characterization under simulated 1 sun conditions. To confirm the reliability of the device fabrication processes, Table 1 also provides the performance of reference devices using ZnO or TiO_2 as ESCs. A comparable PCE of 13.6% was achieved for the ZnO-based devices.[15] For devices using compact TiO_2 (deposited by spray pyrolysis on fluorine-doped tin oxide (FTO)),[10,19] a PCE of 14.2% was attained, which is consistent with previous reports. The statistics of device performance characteristics for Cs_2CO_3-based devices are shown in Supporting Information Figure S2 to ensure the reproducibility of the device fabrication. These results indicated that Cs_2CO_3 treatment on the ITO substrate could achieve efficient electron-selective contact between a perovskite active layer and TCO without the compact n-type metal oxide blocking layers.

For the stability test, the unencapsulated devices were stored in air under ambient conditions (temperature ~20 °C, humidity ~20%) and tested under AM 1.5G simulated 1 sun illumination. Figure 5a shows the stability test results. During the initial 12 h after device fabrication, device efficiency was improved by ~7% due to the increased FF. After 24 h storage, the efficiency decreased sharply because of the decreases in both V_{oc} and FF. For the next 100 h, the efficiency recovered slightly. Compared with the initial performance, the device only showed ~4% decrease in PCE after storage in air for 300 h. These results indicated that the devices based on Cs_2CO_3-modified ITO had similar stability as those using compact TiO_2.[11]

In addition to the device stability, it was also found that electron-selective contact could affect the stability

of $CH_3NH_3PbI_3$ films coated on it. Figure 5b shows the images of $CH_3NH_3PbI_3$ films on Cs_2CO_3-modified or ZnO-coated ITO after annealing treatment. The annealing treatments were performed in a N_2-filled glovebox, and this could eliminate the influence of humidity on the $CH_3NH_3PbI_3$ film. The annealing experiment was first conducted at 130 °C. The film on Cs_2CO_3-modified ITO retained its dark color after 30 min annealing (Figure 5b1). In contrast, the film on ZnO-coated ITO changed color from dark to bright yellow after 5 min annealing (Figure 5b2). Yellow film color indicated the decomposition of $CH_3NH_3PbI_3$, leaving PbI_2 on the substrate.[27−29] $CH_3NH_3PbI_3$ film on ZnO-coated ITO was further examined by annealing at 80 °C. After 1 h annealing, yellow spots could be found in the film, as shown in Figure 5b3, indicating the decomposition of $CH_3NH_3PbI_3$. These results demonstrate that a ZnO-based electron-selective layer may accelerate the decomposition of $CH_3NH_3PbI_3$ film. In contrast, Cs_2CO_3-modified ITO has less negative effect on the stability of $CH_3NH_3PbI_3$, which is similar to those based on TiO_2 electron-selective contacts. However, oxygen vacancies and UV-induced degradation in TiO_2 may also reduce the device's stability.[30]

Interface or surface engineering is often utilized for performance optimization in electronic devices, such as organic solar cells,[31,32] solid-state DSSCs,[33] *etc*. Some recent reports also demonstrated the importance of interfaces in perovskite-based solar cells.[26,30,34,35] A compact electron-selective contact, such as TiO_2 or ZnO, is believed to be a necessary layer for highly efficient perovskite-based solar cells. In the present work, the efficient electron-selective contact was achieved by modifying the ITO surface with Cs_2CO_3 solution. Modification of ITO could tune the surface work function and establish better ohmic contacts between the active layer and ITO,[36,37] leading to efficient device performance. Cesium-based salt materials are the candidates for ITO surface modification. Previous studies have demonstrated that Cs−O bonds could be generated on the ITO surface, which is believed to be the reason for the tuning in the ITO work function.[37,38] In this work, Kelvin probe force microscopy (KPFM) was employed to study the surface potential changes for ITO before or after Cs_2CO_3 treatment (see Figure 3). Results indicated that the surface work function of ITO was 0.4 eV closer to vacuum level after Cs_2CO_3 treatment (as shown in Figure 3c,d). The energy level of ITO, $CH_3NH_3PbI_3$, and Spiro-OMeTAD in Figure 1c is according to the reported literature.[11,36] This could facilitate the electron collection efficiency from the perovskite layer to the TCO substrate. Different from the conventional compact metal oxide electron-selective contacts, Cs_2CO_3 treatment did not form a continuous and compact Cs-based layer; however, the modified ITO surface could realize the function of electron selection. In other words, ITO is tin-doped indium oxide, which is also a compact metal oxide film as the TiO_2 or ZnO. Tin doping in In_2O_3 provides the film with a metallic property. The Cs_2CO_3 treatment on the surface of ITO could tune the surface doping conditions, resulting in electron-selective and hole-blocking functions on the surface of the ITO substrate. Thus, the Cs_2CO_3 treatment of ITO could be understood as the forming of compact n-doped ITO in the surface of bulk ITO film, resulting in the improved ohmic contact between perovskite materials and an ITO conducting substrate.

CONCLUSIONS AND PROSPECTS

In summary, the ITO surface was modified to achieve the efficient electron-selective contacts for perovskite solar cells. This avoided the deposition of compact n-type metal oxide electron-selective layers. The whole device could be fabricated under mild conditions with relative low temperature and solution-based processes. Devices based on the modified ITO surface could achieve a power conversion efficiency exceeding 15%, together with improved device stability under specific conditions. These results imply that interface engineering provides a promising approach to simplify device configuration and reduce the fabrication cost for perovskite solar cells.

METHODS

Materials. All liquid reagents were purchased from Acros and used as received. Cs_2CO_3 and PbI_2 were purchased from Sigma-Aldrich. Spiro-OMeTAD was purchased from SunaTech. CH_3NH_3I was synthesized by CH_3NH_2 with HI according to the reported procedure.[10,11] ZnO nanoparticles were prepared according to literature procedures.[15]

Device Fabrication. The prepatterned ITO substrates (1.5 cm × 1.5 cm, 15 Ω/□) were cleaned with a solution of detergent diluted in deionized water and then rinsed with deionized water, acetone, and 2-propanol. For the devices based on Cs_2CO_3, a 0.5% solution of Cs_2CO_3 (Sigma-Aldrich, Reagent Plus, 99%) in 2-ethoxyethanol (Acros, extra pure, 99%) was spin-coated on the cleaned substrate at 3000 rpm for 30 s and then dried at 150 °C for 1 min. This procedure could be repeated several times according to experiment requirements. The above procedure was finished under ambient conditions (temperature ∼20 °C, humidity ∼20%). A 460 mg·mL^{-1} solution of PbI_2 in *N*,*N*-dimethylformamide was then spin-coated on the Cs_2CO_3-modified substrate (2500 rpm, 15 s) in a N_2 glovebox. After being dried at 100 °C for 10 min, the device was dipped into a CH_3NH_3I solution (10 mg·mL^{-1} in 2-propanol) for 30 s, followed by heating at 130 °C for 30 min in a N_2 glovebox. Subsequently, the Spiro-OMeTAD-based hole-transporting layer (80 mg of Spiro-OMeTAD, 17.5 μL of lithium bis(trifluoromethanesulfonyl)-imide (Li-TFSI) solution (520 mg of Li-TFSI in 1 mL of acetonitrile). and 28.5 μL of 4-*tert*-butylpyridine all dissolved in 1 mL of chlorobenzene) was deposited by spin-coating at 2000 rpm for 30 s in a N_2 glovebox. Finally, the device was completed by depositing a gold electrode (80 nm) through thermal evaporation. For the devices using ZnO on ITO or compact TiO_2 on FTO, the fabrication processes followed the reported methods.[10,15]

Device Characterization. The current–voltage curves were measured using a Keithley 2400 source-measure unit. The cells (active area: 8.5 mm^{-2}) were illuminated by a 150 W class AAA solar simulator (XES-40S1, SAN-EI) equipped with an AM 1.5G filter at a calibrated intensity of 100 $mW \cdot cm^{-2}$. Light intensity was determined by a standard monocrystal silicon photodiode calibrated by the Newport TAC-PV lab. The IPCE spectra were measured in air using a lock-in amplifier coupled with a monochromator (Crowntech, Qtest Station 2000).[15] The light intensity was calibrated by using a standard single-crystal Si photovoltaic cell. All measurements were performed in air at room temperature on the devices without encapsulation (temperature ~20 °C, humidity ~20%).

Other Characterizations. The SEM images were collected by an FEI Nova_NanoSEM 430 field-emission SEM. The AFM images were collected by an Agilent 5500 SPM system (Agilent Technologies, USA). The KPFM measurements were also carried out on the Agilent 5500 SPM system.

Conflict of Interest: The authors declare no competing financial interest.

Acknowledgment. The work was financially supported by the National Natural Science Foundation of China (61377025, 11121091) and the 973 Program of China (2015CB932200). The authors thank Prof. Xinqiang Wang and Mr. Guangbing Wang for the calibration of solar simulator, and Prof. Lixin Xiao for IPCE measurement. R.Z. is grateful to Prof. Yang Yang at UCLA for providing the guide of solar energy research.

Supporting Information Available: Additional SEM images, device performance statics, pictures of the process of Cs_2CO_3-based device fabrication, and photovoltaic performance characterization under different scan conditions. This material is available free of charge *via* the Internet at http://pubs.acs.org.

REFERENCES AND NOTES

1. Gratzel, M.; Janssen, R. A. J.; Mitzi, D. B.; Sargent, E. H. Materials Interface Engineering for Solution-Processed Photovoltaics. *Nature* **2012**, *488*, 304–312.
2. Snaith, H. J. Perovskites: The Emergence of a New Era for Low-Cost, High-Efficiency Solar Cells. *J. Phys. Chem. Lett.* **2013**, *4*, 3623–3630.
3. Park, N. G. Organometal Perovskite Light Absorbers toward a 20% Efficiency Low-Cost Solid-State Mesoscopic Solar Cell. *J. Phys. Chem. Lett.* **2013**, *4*, 2423–2429.
4. McGehee, M. D. Materials Science: Fast-Track Solar Cells. *Nature* **2013**, *501*, 323–325.
5. Xing, G. C.; Mathews, N.; Sun, S. Y.; Lim, S. S.; Lam, Y. M.; Gratzel, M.; Mhaisalkar, S.; Sum, T. C. Long-Range Balanced Electron- and Hole-Transport Lengths in Organic–Inorganic $CH_3NH_3PbI_3$. *Science* **2013**, *342*, 344–347.
6. Gratzel, C.; Zakeeruddin, S. M. Recent Trends in Mesoscopic Solar Cells Based on Molecular and Nanopigment Light Harvesters. *Mater. Today* **2013**, *16*, 11–18.
7. Lotsch, B. V. New Light on an Old Story: Perovskites Go Solar. *Angew. Chem., Int. Ed.* **2014**, *53*, 635–637.
8. Boix, P. P.; Nonomura, K.; Mathews, N.; Mhaisalkar, S. G. Current Progress and Future Perspectives for Organic/Inorganic Perovskite Solar Cells. *Mater. Today* **2014**, *17*, 16–23.
9. Kojima, A.; Teshima, K.; Shirai, Y.; Miyasaka, T. Organometal Halide Perovskites as Visible-Light Sensitizers for Photovoltaic Cells. *J. Am. Chem. Soc.* **2009**, *131*, 6050–6051.
10. Lee, M. M.; Teuscher, J.; Miyasaka, T.; Murakami, T. N.; Snaith, H. J. Efficient Hybrid Solar Cells Based on Meso-Superstructured Organometal Halide Perovskites. *Science* **2012**, *338*, 643–647.
11. Kim, H. S.; Lee, C. R.; Im, J. H.; Lee, K. B.; Moehl, T.; Marchioro, A.; Moon, S. J.; Humphry-Baker, R.; Yum, J. H.; Moser, J. E.; Gratzel, M.; Park, N. G. Lead Iodide Perovskite Sensitized All-Solid-State Submicron Thin Film Mesoscopic Solar Cell with Efficiency Exceeding 9%. *Sci. Rep.* **2012**, *2*, 591.
12. Hodes, G.; Cahen, D. Perovskite Cells Roll Forward. *Nat. Photonics* **2014**, *8*, 87–88.
13. Burschka, J.; Pellet, N.; Moon, S. J.; Humphry-Baker, R.; Gao, P.; Nazeeruddin, M. K.; Gratzel, M. Sequential Deposition as a Route to High-Performance Perovskite-Sensitized Solar Cells. *Nature* **2013**, *499*, 316–319.
14. Liu, M. Z.; Johnston, M. B.; Snaith, H. J. Efficient Planar Hetero Junction Perovskite Solar Cells by Vapor Deposition. *Nature* **2013**, *501*, 395–398.
15. Liu, D. Y.; Kelly, T. L. Perovskite Solar Cells with a Planar Heterojunction Structure Prepared Using Room-Temperature Solution Processing Techniques. *Nat. Photonics* **2014**, *8*, 133–138.
16. Wojciechowski, K.; Saliba, M.; Leijtens, T.; Abate, A.; Snaith, H. J. Sub-150 °C Processed Meso-Superstructured Perovskite Solar Cells with Enhanced Efficiency. *Energy Environ. Sci.* **2014**, *7*, 1142–1147.
17. Research Cell Efficiency Records. NREL (http://www.nrel.gov/ncpv/).
18. Kim, H. S.; Im, S. H.; Park, N. G. Organolead Halide Perovskite: New Horizons in Solar Cell Research. *J. Phys. Chem. C* **2014**, *118*, 5615–5625.
19. Bach, U.; Lupo, D.; Comte, P.; Moser, J. E.; Weissortel, F.; Salbeck, J.; Spreitzer, H.; Gratzel, M. Solid-State Dye-Sensitized Mesoporous TiO_2 Solar Cells with High Photon-to-Electron Conversion Efficiencies. *Nature* **1998**, *395*, 583–585.
20. Eperon, G. E.; Burlakov, V. M.; Goriely, A.; Snaith, H. J. Neutral Color Semitransparent Microstructured Perovskite Solar Cells. *ACS Nano* **2014**, *8*, 591–598.
21. Chen, Q.; Zhou, H. P.; Hong, Z. R.; Luo, S.; Duan, H. S.; Wang, H. H.; Liu, Y. S.; Li, G.; Yang, Y. Planar Heterojunction Perovskite Solar Cells *via* Vapor-Assisted Solution Process. *J. Am. Chem. Soc.* **2014**, *136*, 622–625.
22. Wang, J. T. W.; Ball, J. M.; Barea, E. M.; Abate, A.; Alexander-Webber, J. A.; Huang, J.; Saliba, M.; Mora-Sero, I.; Bisquert, J.; Snaith, H. J.; Nicholas, R. J. Low-Temperature Processed Electron Collection Layers of Graphene/TiO_2 Nanocomposites in Thin Film Perovskite Solar Cells. *Nano Lett.* **2014**, *14*, 724–730.
23. Son, D. Y.; Im, J. H.; Kim, H. S.; Park, N. G. 11% Efficient Perovskite Solar Cell Based on ZnO Nanorods: An Effective Charge Collection System. *J. Phys. Chem. C* **2014**, *118*, 16567–16573.
24. Zhang, Q.; Dandeneau, C. S.; Zhou, X.; Cao, G. ZnO Nanostructures for Dye-Sensitized Solar Cells. *Adv. Mater.* **2009**, *21*, 4087–4108.
25. Docampo, P.; Ball, J. M.; Darwich, M.; Eperon, G. E.; Snaith, H. J. Efficient Organometal Trihalide Perovskite Planar-Heterojunction Solar Cells on Flexible Polymer Substrates. *Nat. Commun.* **2013**, *4*, 2761.
26. Juarez-Perez, E. J.; Wussler, M.; Fabregat-Santiago, F.; Lakus-Wollny, K.; Mankel, E.; Mayer, T.; Jaegermann, W.; Mora-Sero, I. Role of the Selective Contacts in the Performance of Lead Halide Perovskite Solar Cells. *J. Phys. Chem. Lett.* **2014**, *5*, 680–685.
27. Supasai, T.; Rujisamphan, N.; Ullrich, K.; Chemseddine, A.; Dittrich, T. Formation of a Passivating $CH_3NH_3PbI_3/PbI_2$ Interface during Moderate Heating of $CH_3NH_3PbI_3$ Layers. *Appl. Phys. Lett.* **2013**, *103*, 183906.
28. Dualeh, A.; Tétreault, N.; Moehl, T.; Gao, P.; Nazeeruddin, M. K.; Grätzel, M. Effect of Annealing Temperature on Film Morphology of Organic–Inorganic Hybrid Pervoskite Solid-State Solar Cells. *Adv. Funct. Mater.* **2014**, *24*, 3250–3258.
29. Niu, G.; Li, W.; Meng, F.; Wang, L.; Dong, H.; Qiu, Y. Study on the Stability of $CH_3NH_3PbI_3$ Films and the Effect of Post-modification by Aluminum Oxide in All-Solid-State Hybrid Solar Cells. *J. Mater. Chem. A* **2014**, *2*, 705–710.
30. Leijtens, T.; Eperon, G. E.; Pathak, S.; Abate, A.; Lee, M. M.; Snaith, H. J. Overcoming Ultraviolet Light Instability of Sensitized TiO_2 with Meso-Superstructured Organometal Tri-halide Perovskite Solar Cells. *Nat. Commun.* **2013**, *4*, 2885.
31. Chen, L. M.; Xu, Z.; Hong, Z. R.; Yang, Y. Interface Investigation and Engineering: Achieving High Performance Polymer Photovoltaic Devices. *J. Mater. Chem.* **2010**, *20*, 2575–2598.

32. He, Z. C.; Zhong, C. M.; Huang, X.; Wong, W. Y.; Wu, H. B.; Chen, L. W.; Su, S. J.; Cao, Y. Simultaneous Enhancement of Open-Circuit Voltage, Short-Circuit Current Density, and Fill Factor in Polymer Solar Cells. *Adv. Mater.* **2011**, *23*, 4636–4643.
33. Zhu, R.; Jiang, C. Y.; Liu, B.; Ramakrishna, S. Highly Efficient Nanoporous TiO_2—Polythiophene Hybrid Solar Cells Based on Interfacial Modification Using a Metal-Free Organic Dye. *Adv. Mater.* **2009**, *21*, 994–1000.
34. Snaith, H. J.; Abate, A.; Ball, J. M.; Eperon, G. E.; Leijtens, T.; Noel, N. K.; Stranks, S. D.; Wang, J. T.-W.; Wojciechowski, K.; Zhang, W. Anomalous Hysteresis in Perovskite Solar Cells. *J. Phys. Chem. Lett.* **2014**, *5*, 1511–1515.
35. Schulz, P.; Edri, E.; Kirmayer, S.; Hodes, G.; Cahen, D.; Kahn, A. Interface Energetics in Organo-Metal Halide Perovskite-Based Photovoltaic Cells. *Energy Environ. Sci.* **2014**, *7*, 1377–1381.
36. Li, G.; Chu, C. W.; Shrotriya, V.; Huang, J.; Yang, Y. Efficient Inverted Polymer Solar Cells. *Appl. Phys. Lett.* **2006**, *88*, 253503.
37. Liao, H. H.; Chen, L. M.; Xu, Z.; Li, G.; Yang, Y. Highly Efficient Inverted Polymer Solar Cell by Low Temperature Annealing of Cs_2CO_3 Interlayer. *Appl. Phys. Lett.* **2008**, *92*, 173303.
38. Cheng, G.; Tong, W. Y.; Low, K. H.; Che, C. M. Thermal-Annealing-Free Inverted Polymer Solar Cells Using ZnO/Cs_2CO_3 Bilayer as Electron-Selective Layer. *Sol. Energy Mater. Sol. Cells* **2012**, *103*, 164–170.